IEEE Access
Multidisciplinary | Rapid Review | Open Access Journal

Received April 7, 2021, accepted May 21, 2021, date of publication May 26, 2021, date of current version June 7, 2021.

Digital Object Identifier 10.1109/ACCESS.2021.3083810

Control Strategy and Experimental Research of Cable-Driven Lower Limb Rehabilitation Robot

YAN-LIN WANG, KE-YI WANG, XIANG LI, ZONG-JUN MO, AND KUI-CHENG WANG
College of Mechanical and Electrical Engineering, Harbin Engineering University, Harbin 150001, China

Corresponding authors: Ke-Yi Wang (wangkeyi@hrbeu.edu.cn) and Yan-Lin Wang (wangyanlin0513@21cn.com)

This work was supported in part by the National Natural Science Foundation of China under Grant 51405095, in part by the Natural Science Foundation of Heilongjiang Province, China, under Grant LH2019E032, in part by the Postdoctoral Scientific Research Fund of Heilongjiang under Grant LBH-Q15030, and in part by the Fundamental Research Funds for the Central Universities of the Harbin Engineering University under Grant 3072019CF0704.

ABSTRACT The passive training with fixed trajectory is more suitable for the initial rehabilitation training of patients with no muscle strength in the affected limb. In order to meet the needs of patients' rehabilitation training in different rehabilitation stages and improve the active participation and rehabilitation training effect of patients, a fuzzy sliding mode variable admittance (FSMVA) controller based on safety evaluation and supervision is proposed for the cable-driven lower limb rehabilitation robot (CDLR) in this paper. The FSMVA controller consists of an inner loop fuzzy sliding mode controller, an outer loop variable admittance controller, and a safety evaluation and supervision module. Through the safety evaluation index of the CDLR system and the comprehensive evaluation of patients' rehabilitation effect given by rehabilitation physiotherapists, a real-time adjustment algorithm of variable admittance controller parameters is designed, which can realize the real-time switching of training modes and adjustment of variable admittance controller parameters in active training mode and passive training mode. The trajectory tracking experiments with no admittance, fixed admittance, and variable admittance based on safety evaluation and supervision were carried out on the experimental platform. The experimental results show that the proposed FSMVA control strategy has high position control accuracy in the active training mode. In addition, the training intensity and the active participation of patients can be increased according to the patient's exercise ability. In the passive training mode, according to the training needs of patients, the amount of the trajectory adjustment can be increased to improve the comfort of the training process and the safety of patients. It lays a foundation for the further study of the evaluation system of the rehabilitation training process and the experiment of human-machine interaction compliance.

INDEX TERMS Lower limb rehabilitation, rehabilitation training, fuzzy sliding mode control, variable admittance control, safety evaluation and supervision.

I. INTRODUCTION

With the acceleration of global aging, the number of patients with lower limb dyskinesia caused by disease and functional degradation has been increasing. Clinical medical research shows that the movement function of patients' limbs can be recovered and the movement ability of patients' limbs can be improved by scientific high-intensity and repetitive training [1], [2]. At present, the global medical resources are seriously inadequate, causing many patients to unable to receive rehabilitation treatment and finally lose their movement function. Therefore, the robot technology has been well applied to the rehabilitation field to help patients receive scientific and effective rehabilitation training, which has become the forefront of robot technology research [3], [4].

Rehabilitation robot is a research achievement in multidisciplinary fields, such as rehabilitation medicine, biomechanics, mechanics, and automatic control, and so on. At present, according to the structural characteristics, the lower limb rehabilitation robots mainly include two kinds, exoskeleton type and parallel end-effector-based cable-driven rehabilitation devices (CDRDs) type [5], [6]. The exoskeleton rehabilitation devices have a strict corresponding relationship between the joints of the robot and the human limbs, which can realize the coordinated movement training of multiple joints and the independent movement training

The associate editor coordinating the review of this manuscript and approving it for publication was Her-Terng Yau.

of single joints, and have strong training pertinence. The typical application cases are: CAREX-7 (a 7 DOFs cable-driven arm exoskeleton studied by Beihang University) [7], 6 DOFs LLE (lower limb exoskeleton studied by University Kebangsaan Malaysia) [8], [9], LLWRE (a lower limb wearable robotic exoskeleton studied by University of Iceland) is an exoskeleton lower limb rehabilitation robot studied by Harvard University [10], and so on. However, the exoskeleton type rehabilitation devices have some problems, such as the structure is complex, the training form is single, the motion error is large, the man-machine compatibility is poor, and so on [12], [13]. Compared with the exoskeleton type rehabilitation robot, the parallel end-effector-based CDRDs can realize the rehabilitation training of human limbs generally driven by cable, which has the following advantages, such as the structure is simple, the reliability is high, the reconstruction ability is strong, the man-machine compatibility is better, and the system stiffness can be adjusted. These characteristics make it well applied in the rehabilitation field [14], [15]. Zou YP *et al.* designed a mobile lower limb rehabilitation robot driven by four cables, in which two cables drive the ankle joint of the lower limb and the other two cables drive the knee joints of the lower limb [16], [17]. But four cables are arranged in the same vertical plane, the training form of the lower limb will be relatively simple. Giacomo Z. *et al.* designed a parallel exoskeleton-based CDRD [18]. However, the robot can only complete exercise training with a single degree of freedom of the limb. Matteo R. *et al.* designed a cable-driven ankle rehabilitation robot based on the cable-driven S-4SPS parallel architecture [19], which has greater motion assistance range than the motion range of human ankle in normal walking gait. Zi B. *et al.* designed a cable-driven parallel robot for waist rehabilitation training. A platform on which patients stand is driven by cables to realize the waist rehabilitation training [20]. Giuseppe C. *et al.* designed a novel cable-driven parallel robot for the assistance of patients in rehabilitation training of both upper and lower limbs without having to disassemble any part of the structure [21]. Wang Y.L. and Wang K.Y. *et al.* designed a rigid-flexible hybrid-driven lower limb gait training robot. The rigid motion module is introduced into the motion branch chain of the CDLR, which not only increases the diversity of lower limb gait training form, but also improves the movement flexibility of the rehabilitation robot [22], [23]. The rehabilitation robot is a very complicated man-machine coupling system. Hence, the control method of this kind of the system is difficult. Many scholars have proposed different trajectory tracking control strategies to improve the accuracy of system in passive training. Zhang L.X. and Wang Y.L. *et al.* proposed a compound controller based on modern control theory to eliminate the surplus force caused by the motion of the end-effector and external interference [24], [25], which effectively improve the loading accuracy of the tension force of the cable-driven units. Zi B. *et al.* designed a two-level control algorithm based on the fuzzy algorithm and PID algorithm. The position tracking of the end-effector is realized through the PID controller, and the PID controller parameters can be adjusted by the fuzzy algorithm according to the change of cable tensions to ensure the safety of the patient [20]. In addition, the robust adaptive control method [26], sliding mode control method [27], [28], and force-position control method [29] were studied to realize position tracking control of the robot.

In different rehabilitation stages, the exercise strength that the lower limb muscles can provide is different. In the middle and later stages of patients' rehabilitation training, the active training mode should take the patients' active movement intention and ability into account in the rehabilitation training so as to improve the active participation enthusiasm and training effect of patients' in training. Pehlivan *et al.* proposed a minimum assist-as-needed controller, which allows patients to make use of the recovered muscle strength of the lower limb during training, to the greatest extent [30]. Banala *et al.* designed an adaptive force domain controller to adjust the human-machine interaction force and the active participation of patients in training according to the motion error of the ankle joint [31]. Jun J. *et al.* proposed a hybrid force-position control algorithm for cable-driven parallel robots (CDPR), which can modify the expected position of the end-effector according to the force spinor [32]. M. H. Korayem *et al.* designed a robust feedback linearization control approach based on the path planning of a cable-suspended robot [33]–[35]. Mehran R. *et al.* designed a novel fuzzy sliding mode control for the exoskeleton robot, which is robust against external disturbances and unknown dynamics [36]. Fortin-Cote, An *et al.* proposed a speed closed-loop admittance control algorithm for the CDPR. The speed of the end-effector can be adjusted by the admittance controller [37]. Yang Q. *et al.* designed an admittance controller for the cable-driven upper limb rehabilitation robot, which can modify the desired trajectory according to the interaction force between the patient and the end-effector [38]. The above control strategies can achieve different degrees of training effects. In the published papers, there are few studies on the automatic switching between active training mode and passive training mode, real-time adjustment of patients' training intensity, and the safety of the CDLR and the CDPR. Therefore, the admittance control strategy reported in the existing literature can't be used in the whole rehabilitation training process of patients.

For patients who have recovered part muscle strength, the passive position control strategy didn't take into account the patient's active participation in the rehabilitation training, so it can't meet the training needs of this kind of patients very well.

The admittance control strategy with fixed admittance didn't take into account the exercise ability of patients, which will affect the comfort and safety of patients in the training and the enthusiasm of patients to participate actively. Therefore, a CDLR is designed in this paper, and a FSMVA control strategy is proposed based on the safety evaluation of the CDLR system. In this study, the designed admittance

controller parameters can be adjusted in real-time according to the safety evaluation index of the CDLR system in the current moment and the comprehensive evaluation of the rehabilitation effect given by rehabilitation physiotherapists. Furthermore, the training intensity can be adjusted to meet the training needs of patients in different rehabilitation training stages and effectively improve the efficiency of rehabilitation training. It provides a basis for further study of the rehabilitation evaluation system and optimization of controller parameters and man-machine compliance experiments.

II. CDLR

The CDLR can help patients perform different forms of rehabilitation training through the coordinated movement of cable motion chains. For example, in the initial rehabilitation stage, the lower limb muscles of patients can't provide enough force for the basic movement of lower limbs. Therefore, cables are required to provide the force for the training of lower limb according to pre-set trajectory to prevent degeneration of muscle function of lower limbs. This mode is called passive training mode. In the middle and later rehabilitation training stages, the lower limb muscles of the patient can provide part or all of the strength required for the exercise. At this time, the CDLR only needs to provide some insufficient forces of the lower extremity or follow the lower limb to complete the rehabilitation training. This training mode is called assistant training mode or active training mode. Besides, different compound motion forms need to be completed in training.

In order to achieve multi-mode and diversified rehabilitation training, a CDLR is designed, as shown in Fig. 1, which mainly consists of four cable-drives units (CDU), a position sensor, an end-effector (i.e. lower limb traction point), control cabinet, and frame. 3-D model of the CDLR is shown in Fig. 1(a). The preliminary scaled prototype experimental system is shown in Fig. 1(b).

The CDU is shown in Fig. 1(b(II)). One end of the cable is fixed at the ankle of the prosthetic limb(or end-effector). The other end of the cable is connected on roller via pulley and tension sensor. The roller is fixed on the output shaft of the torque motor integrated with photoelectric encoder. The cable tension data are collected by tension sensors with an amplifier. Furthermore, the height of pulley b_i in Fig. 1(a) can be adjusted by a slider screw mechanism to meet the requirements of different patients and training tasks.

The end-effector is shown in Fig. 1(b(III)). An infrared reflection bracket with 3 infrared reflectors is installed at the end-effector.

The position sensor is shown in Fig. 1(b(IV)). The position sensor can emit 4 sets of infrared rays at the same time, which are reflected by the infrared reflection bracket in Fig. 1(b(III)), and then the sensor detects the infrared rays to calculate the spatial position of the end-effector. The position data is directly uploaded to the host computer to store the motion state of the end-effector and realize the motion control of the CDLR.

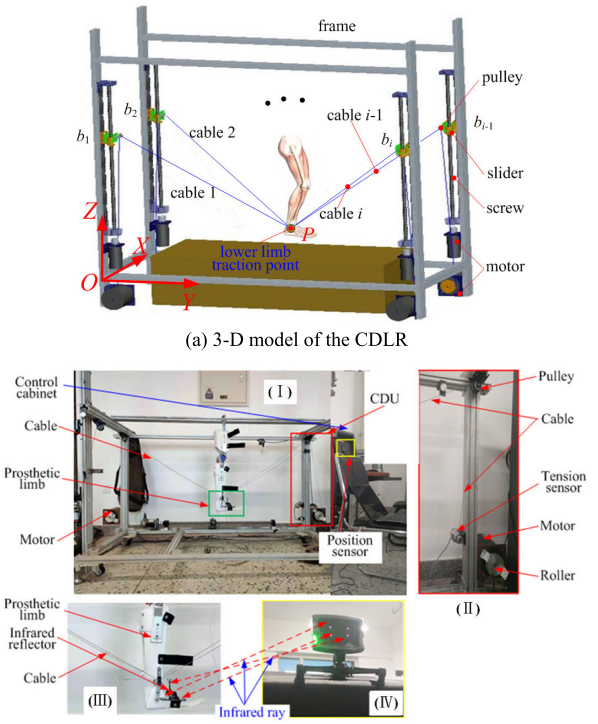

(a) 3-D model of the CDLR

(b) Preliminary scaled prototype experimental system

FIGURE 1. CDLR.

As shown in Fig. 1(b(I)), the control cabinet is integrated with an industrial computer, a motion control card, four drivers, a data acquisition card, and a power supply.

In the actual training process, the height of the pulley b_i can be set according to the height of patients and the needs of the training task through the screw slider mechanism. Of course, the height of pulley b_i can be adjusted in real-time according to the pre-planned training task during the training process. The motion instructions of the CDU are sent through the industrial computer and the motion control card, and the motion of the lower limb can be realized by CDUs. In addition, the position data of the traction point are collected via the position sensor. The cable tensions data are collected via the tension sensors. The position data and the cable tensions data are fed back to the industrial computer. The movement training of the lower limbs can be accurately or compliantly controlled via the designed controller. Then the closed-loop control of lower limb rehabilitation training is realized.

III. MECHANICS ANALYSIS

The configuration of the CDLR is shown in Fig. 1(a), in the global coordinate system $O - XYZ$, $\boldsymbol{L}_i (i = 1, 2, 3, 4)$ is the length vector of cable L_i. (x_i, y_i, z_i) is the position of the pulley b_i. $\boldsymbol{X} = (x, y, z)$ is the position of the lower limb traction point P. According to the principle of vector closure, the length vector of cable can be written as:

$$\boldsymbol{L}_i = \boldsymbol{O}\boldsymbol{b}_i - \boldsymbol{O}\boldsymbol{P} \quad (i = 1, 2, 3, 4) \tag{1}$$

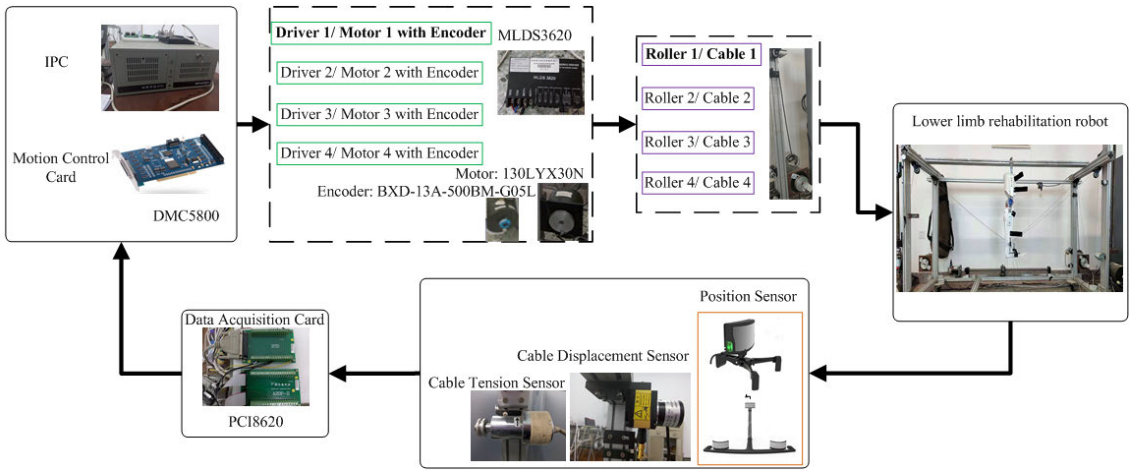

FIGURE 2. Frame diagram of the CDLR's control system.

Hence, the length of cable L_i can be written as:

$$L_i = \|\boldsymbol{L}_i\| = \sqrt{(\boldsymbol{Ob}_i - \boldsymbol{OP})\,(\boldsymbol{Ob}_i - \boldsymbol{OP})^{\mathrm{T}}} \tag{2}$$

In addition, $\boldsymbol{\theta} = [\theta_1, \theta_2, \theta_3, \theta_4]^{\mathrm{T}}$ indicates angles of the motor. $\boldsymbol{r} = [r_1, r_2, r_3, r_4]^{\mathrm{T}}$ indicates the transfer coefficient between the angle of the motor and the change in cable length, that is the radius of the roller. So the length vector of cable can be further written as:

$$\boldsymbol{L} = \boldsymbol{L}_0 + \boldsymbol{r} \cdot \boldsymbol{\theta} \tag{3}$$

where $\boldsymbol{L}_0$ indicates the initial length vector of the cables.

In the rehabilitation training, the lower limb is driven by the cable tension forces to complete the training task. According to the Euler-Lagrange equations, the dynamics equation of the end-effector can be expressed as:

$$\boldsymbol{J}^{\mathrm{T}}\boldsymbol{T} + \boldsymbol{W} = \boldsymbol{0} \tag{4}$$

where $\boldsymbol{T} = [t_1, t_2, t_3, t_4]^{\mathrm{T}}$ indicates cable tensions, $\boldsymbol{W}$ presents external forces acting on end-effector (including self-weight of end-effector).

EQ. (4) can be further expressed as:

$$\boldsymbol{M}(\boldsymbol{X})\ddot{\boldsymbol{X}} + \boldsymbol{N}(\boldsymbol{X}, \dot{\boldsymbol{X}})\dot{\boldsymbol{X}} + \boldsymbol{G} + \boldsymbol{W}_{\boldsymbol{e}} = \boldsymbol{J}^{\mathrm{T}}\boldsymbol{T} \tag{5}$$

where $\boldsymbol{M}(\boldsymbol{X})$ indicates the inertial matrix of the CDLR. $\boldsymbol{N}(\boldsymbol{X}, \dot{\boldsymbol{X}})$ indicates the Coriolis matrix of the CDLR. $\boldsymbol{G}$ indicates the gravity vector of the end-effector. $\boldsymbol{W}_e$ indicates unknown external interference and modeling errors. $\boldsymbol{J}^{\mathrm{T}}$ indicates the Jacobian matrix of the CDLR. $\dot{\boldsymbol{X}} = (\dot{x}, \dot{y}, \dot{z})$ and $\ddot{\boldsymbol{X}}$ indicate the velocity and acceleration of the end-effector, respectively.

The length and tension of the cable are controlled via the roller driven by the motor. In order to improve the control accuracy of the rehabilitation robot, it is necessary to consider the dynamics of the driven unit in the dynamic analysis. The driven unit consists of a motor and a roller. So the dynamics of the driven unit can be expressed as:

$$\boldsymbol{J}_{\boldsymbol{m}}\ddot{\boldsymbol{\theta}} + \boldsymbol{B}_{\boldsymbol{m}}\dot{\boldsymbol{\theta}} + \boldsymbol{r}\boldsymbol{T} = \boldsymbol{\tau} \tag{6}$$

where $\boldsymbol{J}_{\boldsymbol{m}} = diag(J_{m1}, J_{m2}, J_{m3}, J_{m4})$, and J_{mi} indicates the equivalent rotation inertia of the motor rotor and the roller. $\boldsymbol{B}_{\boldsymbol{m}} = diag(B_{m1}, B_{m2}, B_{m3}, B_{m4})$, and B_{mi} indicates the equivalent viscous damping coefficient of the motor rotor and the roller. $\boldsymbol{\tau} = [\tau_1, \tau_2, \tau_3, \tau_4]^{\mathrm{T}}$, and τ_i indicates the output torque of the i^{th} motor. $\dot{\boldsymbol{\theta}}$ and $\ddot{\boldsymbol{\theta}}$ indicates the angle velocity and angle acceleration of the roller. $\boldsymbol{r}$ is the radius of the roller.

It can be known from EQs. (2) and (3) that the rotation angle of the motor is:

$$\boldsymbol{\theta} = \boldsymbol{r}^{-1}(\boldsymbol{L} - \boldsymbol{L}_0) \tag{7}$$

The relation between the speed of the roller and speed of end-effector can obtain via first order differential for time of EQ. (7), which can be written as:

$$\dot{\boldsymbol{\theta}} = \boldsymbol{r}^{-1}\dot{\boldsymbol{L}} = \boldsymbol{r}^{-1}\boldsymbol{J}\dot{\boldsymbol{X}} \tag{8}$$

So, their acceleration relation can be expressed as:

$$\ddot{\boldsymbol{\theta}} = \boldsymbol{r}^{-1}\boldsymbol{J}\ddot{\boldsymbol{X}} + \boldsymbol{r}^{-1}\dot{\boldsymbol{J}}\dot{\boldsymbol{X}} \tag{9}$$

Substituting EQs. (6), (8), and (9) into EQ. (5), one can obtain the system dynamics equation of the CDLR as follows:

$$\boldsymbol{M}_{eq}(\boldsymbol{X})\ddot{\boldsymbol{X}} + \boldsymbol{N}_{eq}(\boldsymbol{X}, \dot{\boldsymbol{X}})\dot{\boldsymbol{X}} + \boldsymbol{G}_{eq} + \boldsymbol{W}_e = \boldsymbol{J}^{\mathrm{T}}\boldsymbol{\tau} \tag{10}$$

where:

$$\begin{cases} \boldsymbol{M}_{eq}(\ddot{\boldsymbol{X}}) = \boldsymbol{r}\boldsymbol{M}(\boldsymbol{X}) + \boldsymbol{J}^{\mathrm{T}}\boldsymbol{J}_{\boldsymbol{m}}\boldsymbol{r}^{-1}\boldsymbol{J} \\ \boldsymbol{N}_{eq}(\boldsymbol{X}, \dot{\boldsymbol{X}}) = \boldsymbol{r}\boldsymbol{N}(\boldsymbol{X}, \dot{\boldsymbol{X}}) + \boldsymbol{r}^{-1}\boldsymbol{J}^{\mathrm{T}}\boldsymbol{J}_{\boldsymbol{m}}\dot{\boldsymbol{J}} + \boldsymbol{r}^{-1}\boldsymbol{J}^{\mathrm{T}}\boldsymbol{B}_{\boldsymbol{m}}\boldsymbol{J} \\ \boldsymbol{G}_{eq} = \boldsymbol{r}\boldsymbol{G} \end{cases} \tag{11}$$

IV. DESIGN OF THE FUZZY SLIDING MODE VARIABLE ADMITTANCE CONTROLLER

The CDLR's control system consists of a position sensor, four tension sensors, a data acquisition card, a motion control card, four drivers, and four torque motors with integrated photoelectric encoder. The frame diagram of the CDLR's control system is shown in Fig. 2. The position data of

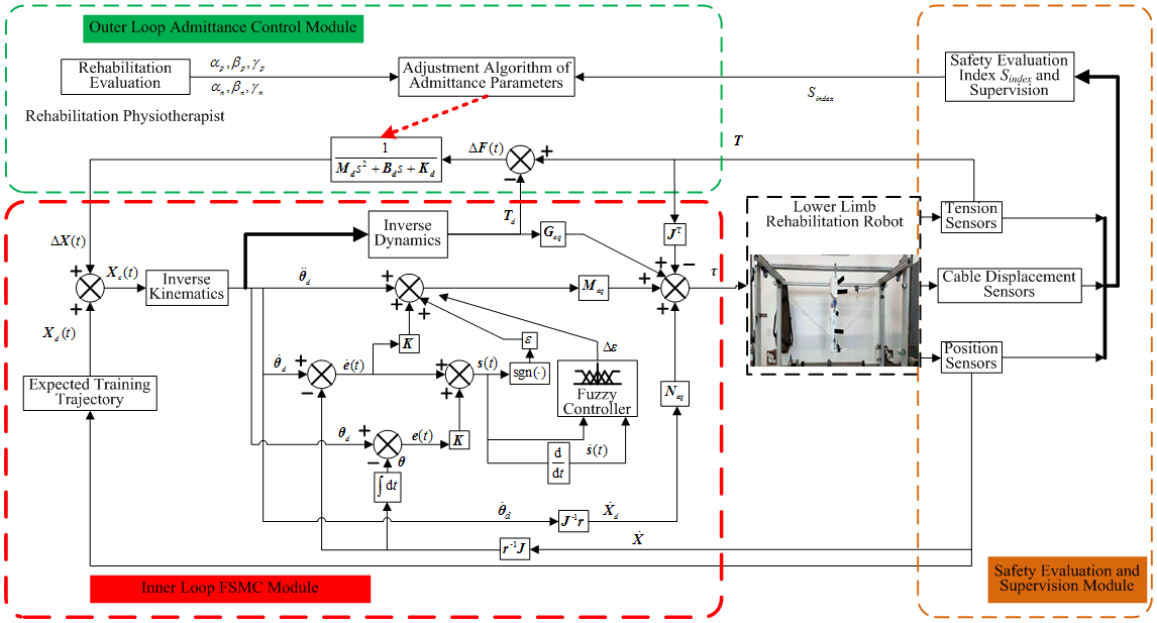

FIGURE 3. Schematic of the proposed FSMVA control strategy for the CDLR.

the traction point are collected via the position sensor. The cable tensions data are collected via the tension sensors. The industrial personal computer (IPC) and motion control card can generate a control signals and send them to the drivers. In order to meet the training needs of different patients in different rehabilitation stages and ensure the safety of patients, this study introduces the safety evaluation and supervision module and the rehabilitation physiotherapist optimization parameters module into the control system to protect the patient and improve the training effect.

In order to meet the needs of rehabilitation training tasks of patients with different movement disorders in different rehabilitation stages, a FSMVA algorithm is proposed for the CDLR, which considers the safety of the CDLR system. In the rehabilitation training, the compliance of human-machine interaction can be adjusted by changing the admittance parameters of the FSMVA controller, and the active training mode can be changed from the passive training mode to realize the active training with different intensity. The schematic of the proposed FSMVA control strategy for the CDLR is shown in Fig. 3, which includes the outer loop admittance control module, the inner loop fuzzy sliding mode control (FSMC) module, and the safety evaluation supervision module.

The outer loop admittance control module is to establish a relationship between the interaction force, between the lower limbs of the human and the CDLR, and the adjustment amount of the tracking trajectory in rehabilitation training. Patients can adjust the training intensity in real-time according to their active exercise ability in the rehabilitation training process. The admittance parameters of the admittance controller can be optimized based on the safety evaluation index of the CDLR, the rehabilitation stages and rehabilitation effect of patients, and the clinical experience of rehabilitation physiotherapists. The inner loop FSMC module is used to realize the precise control of the training trajectory and the adjustment amount of the training trajectory for the CDLR. The safety evaluation and supervision module is used to calculate the safety evaluation index and supervise the motion state of the CDLR system. When the training state is in an unsafe state, the movement of the CDLR will be stopped immediately to ensure the safety of patients. The safety evaluation index of the CDLR system has been discussed in detail by the author in the literature [39] and [41], so this paper directly uses the safety evaluation algorithm in the literature [39] and [41].

According to the admittance control principle, the target admittance model of the end-effector of the CDLR in the global coordinate system can be expressed as:

$$\begin{cases} \Delta \boldsymbol{F}(t) = \boldsymbol{M_d}\Delta\ddot{\boldsymbol{X}}(t) + \boldsymbol{B_d}\Delta\dot{\boldsymbol{X}}(t) + \boldsymbol{K_d}\Delta\boldsymbol{X}(t) \\ \Delta \boldsymbol{F}(t) = \boldsymbol{F}(t) - \boldsymbol{F}_d(t) \\ \Delta \boldsymbol{X}(t) = \boldsymbol{X}_c(t) - \boldsymbol{X_d}(t) \end{cases} \tag{12}$$

where $\boldsymbol{M_d}$, $\boldsymbol{B_d}$, and $\boldsymbol{K_d}$ indicate the target inertia matrix, target damping matrix, and target stiffness matrix, respectively. $\boldsymbol{F}_d(t)$, $\boldsymbol{F}(t)$, and $\Delta\boldsymbol{F}(t)$ respectively represent the expected interaction force, actual interaction force, and deviation between the expected interaction force and the actual interaction force. $\boldsymbol{X_d}(t)$, $\boldsymbol{X}_c(t)$, and $\Delta\boldsymbol{X}(t)$ respectively represent the expected motion trajectory, actual motion trajectory, and adjustment amount of motion trajectory of the end- effector of the CDLR.

In the actual training process, the safety of the rehabilitation robot to the patient must be guaranteed. Therefore, this paper establishes a safety evaluation and supervision module based on the safety evaluation index S_{index} of the CDLR system proposed in the literature [39], [41] in the control system. Combined with the clinical experience of the rehabilitation physiotherapist, the admittance parameters of the admittance controller can be adjusted and optimized according to the comprehensive evaluation for the rehabilitation stage and rehabilitation effect of patients given by the rehabilitation physiotherapist. The adjustment algorithm of the admittance parameters of the admittance controller can be expressed as (13), shown at the bottom of the page, where $\boldsymbol{M_{da0}}, \boldsymbol{M_{dp0}}, \boldsymbol{B_{da0}}, \boldsymbol{B_{dp0}}, \boldsymbol{K_{da0}}$, and $\boldsymbol{K_{dp0}}$ respectively represent the desired target inertia matrix, the desired target damping matrix, and the desired target stiffness matrix in active and passive training modes. The detail calculation process of the safety evaluation index S_{index} of the CDLR is in references [39] and [41]. The parameters α_a and α_p represent the rate of change of the target inertia matrix $\boldsymbol{M_d}$ manually adjusted by the rehabilitation physiotherapist in the active training mode and passive training mode respectively; the parameters β_a and β_p represent the rate of change of the target damping matrix $\boldsymbol{B_d}$ manually adjusted by the rehabilitation physiotherapist in the active training mode and passive training mode respectively; the parameters γ_a and γ_p represent the rate of change of the target damping matrix $\boldsymbol{K_d}$ manually adjusted by the rehabilitation physiotherapist in the active training mode and passive training mode respectively. The safety evaluation index S_{index} of the CDLR can be written as [39], [41]:

$$S_{index} = \left(\eta_{TP}\frac{T^P_{\min}}{T^P_{\max}} + \eta_{KP}\frac{\sigma_{P\min}}{\sigma_{P\max}}\right)\cdot\left(\eta_T\frac{T^P_{\min}}{T^{\min}_{\max}} + \eta_K\frac{\sigma_{P\min}}{\sigma^{\min}_{\max}}\right)\cdot\left(\eta_{Pv}\frac{\tan\theta_P}{\tan\theta_Q} + \eta_{Ph}\frac{\tan\theta_M}{\tan\theta_Q}\right)\cdot\left(1-\frac{v_P}{v_{\max}}\right) \quad (14)$$

where $T^P_{\min}, T^P_{\max}$ and $T^{\min}_{\max}$ respectively indicate the minimum value, the maximum value of the tension force of cables at the current position, and the maximum value of the minimum tension forces of cables in the workspace. $\sigma_{P\min}, \sigma_{P\max}$ and $\sigma^{\min}_{\max}$ respectively represent the minimum singular value and the maximum singular value of the system stiffness matrix at the current position, and the maximum value of the minimum singular value of the system stiffness matrix in the workspace. θ_P, θ_Q, and θ_M indicate the angle θ when the traction point is at any position, the center points of the horizontal section where the traction point is located at any position and the upper surface of the workspace, respectively. v_P and $v_{\max}$ respectively indicate the movement speed of the traction point at any position and the maximum allowable safe speed determined by the patient's motion tolerance ability.

When calculating the safety evaluation index of the CDLR system, it is necessary to determine the weight coefficients according to the size of the contributions of all performance factors to the safety [39], [41]. Specifically, the weighted coefficients η_{TP} and η_{kP} reflect the size of the contribution of $\wp_{TP}$ and $\wp_{kP}$ to the safety, respectively. $\wp_{TP}$ and $\wp_{kP}$ indicate the distribution uniformity of the cable tension and the system stiffness in each direction at the current position. The relationship between the system stiffness and the cable tension shows the cable tension is one of the important factors for determining the system stiffness of the CDLR, and the cable tension is the direct factor that drives the lower limb motion and resists external interference. Hence, the cable tension performance factor $\wp_{TP}$ is more important than the system stiffness performance factor $\wp_{kP}$ at the current position to the safety. Namely, the weighted coefficients meet $\eta_{TP} > \eta_{kP}$. The weighted coefficients η_T and η_k reflect the size of the contribution of $\wp_T$ and $\wp_k$ to the safety, respectively. $\wp_T$ and $\wp_k$ indicate the distribution uniformity of the cable tension and the system stiffness in each direction in the whole workspace; and because of the above same reasons, the cable tension performance factor $\wp_T$ is more important than the system stiffness performance factor $\wp_k$ in the whole workspace to the safety. But the importance here is weaker than $\wp_{TP}$ and $\wp_{kP}$. So, the weighted coefficients meet $\eta_{TP} > \eta_{kP}$; the weighted coefficients η_{pv} and η_{ph} reflect the size of the contribution of $\wp_{pv}$ and $\wp_{ph}$ to the safety, respectively. $\wp_{pv}$ and $\wp_{ph}$ indicate the distance from the current position to the vertical midline and upper surface of the workspace, respectively. When the traction point is closer to the vertical midline of the workspace, the more uniform the distribution of cable tension is, and the more uniform the distribution of system stiffness is. When the traction point is closer to the upper surface of the workspace, the larger the cable tension is, the larger the system stiffness is. However, the distribution uniformity of the cable tension is more important to the safety of rehabilitation robots than the system stiffness to the safety. Hence, $\wp_{pv}$ is more important than $\wp_{ph}$. Namely, the weighted coefficients meet $\eta_{pv} > \eta_{ph}$; According to the CDLR parameters, the robot configuration constraints and the

$$\begin{cases} \boldsymbol{M_d} = \begin{cases} \boldsymbol{M_{da0}} + (1 - S_{index})\alpha_p, & \textit{for active training mode} \\ \boldsymbol{M_{dp0}} - (1 - S_{index})\alpha_n, & \textit{for passive training mode} \end{cases} \\ \boldsymbol{B_d} = \begin{cases} \boldsymbol{B_{da0}} + (1 - S_{index})\beta_p, & \textit{for active training mode} \\ \boldsymbol{B_{dp0}} - (1 - S_{index})\beta_n, & \textit{for passive training mode} \end{cases} \\ \boldsymbol{K_d} = \begin{cases} \boldsymbol{K_{da0}} + (1 - S_{index})\gamma_p, & \textit{for active training mode} \\ \boldsymbol{K_{dp0}} - (1 - S_{index})\gamma_n, & \textit{for passive training mode} \end{cases} \end{cases} \quad (13)$$

optimized performance indicator of the cable tension in the study, the weight coefficients selected in the study are $\eta_{TP} = 0.6$, $\eta_{KP} = 0.4$, $\eta_T = 0.55$, $\eta_K = 0.45$, $\eta_{Pv} = 0.6$, and $\eta_{Ph} = 0.4$ [39], [41].

In addition, the safety evaluation and supervision module should supervise the safety of the CDLR system to ensure the safety of patients in the training process. When the safety evaluation index S_{index} of the CDLR system is smaller than a given value S^*_{index}, the motion state of the system is not safe for patients, so the system should shut down urgently, which can be expressed as:

$$\begin{cases} \text{If} & S_{index} < S^*_{index} \\ \text{then} & \\ & \text{shut down} \\ \text{end} & \end{cases} \tag{15}$$

where the given value S^*_{index} depends on the exercise capacity, the treatment and rehabilitation plan of patients. In this study, $S^*_{index} = 0.01$.

In frequency domain space, EQ. (12) can be further expressed as:

$$\frac{\Delta \boldsymbol{F}(s)}{\boldsymbol{M_d}s^2 + \boldsymbol{B_d}s + \boldsymbol{K_d}} = \Delta \boldsymbol{X}(s) \tag{16}$$

The error of the tracking track is defined as $\boldsymbol{e}(t)$:

$$\boldsymbol{e}(t) = \boldsymbol{\theta}_d(t) - \boldsymbol{\theta}(t) \tag{17}$$

where $\boldsymbol{\theta}_d(t)$ and $\boldsymbol{\theta}(t)$ represent the expected and actual motion angles of the motor, respectively.

The switching function of the sliding surface is designed as follows:

$$\boldsymbol{s}(t) = \boldsymbol{K}\boldsymbol{e}(t) + \dot{\boldsymbol{e}}(t) \tag{18}$$

where $\boldsymbol{s}(t)$ is the slope of the sliding surface. $\boldsymbol{K}$ is the diagonal positive matrix of the proportional term of the switching function.

From EQs. (9), (10), (17), and (18), the first derivative of the slope of the sliding surface with respect to time can be written as follows:

$$\begin{aligned} \dot{\boldsymbol{s}}(t) = \boldsymbol{K}\dot{\boldsymbol{e}}(t) + \ddot{\boldsymbol{\theta}}(t) - \boldsymbol{M}_{eq}^{-1}(\boldsymbol{r}^{-1}\boldsymbol{J}\boldsymbol{J}^{\mathrm{T}}\boldsymbol{\tau} \\ + (\boldsymbol{N}_{eq} - \boldsymbol{M}_{eq}\boldsymbol{J}^{+}\dot{\boldsymbol{J}})\boldsymbol{\theta}(t) - \boldsymbol{r}^{-1}\boldsymbol{J}\boldsymbol{G}_{eq} - \boldsymbol{W}_e) \end{aligned} \tag{19}$$

where $\boldsymbol{J}^+$ is the Moore–Penrose generalized inverse matrix of the matrix $\boldsymbol{J}$, and $\boldsymbol{J}^+ = \boldsymbol{J}^{\mathrm{T}}\left(\boldsymbol{J}\boldsymbol{J}^{\mathrm{T}}\right)^{-1}$.

The sliding mode controller is designed as:

$$\begin{aligned} \boldsymbol{u}(t) = \boldsymbol{M}_{eq\theta}\boldsymbol{K}\dot{\boldsymbol{e}}(t) + \boldsymbol{M}_{eq\theta}\ddot{\boldsymbol{\theta}}(t) + (\boldsymbol{N}_{eq\theta} - \boldsymbol{M}_{eq\theta}\boldsymbol{J}^{+}\dot{\boldsymbol{J}})\boldsymbol{\theta}(t) \\ - \boldsymbol{G}_{eq\theta} + \boldsymbol{M}_{eq\theta}\boldsymbol{\varepsilon} \cdot \mathrm{sgn}(\boldsymbol{s}(t)) \end{aligned} \tag{20}$$

where $\mathrm{sgn}(\cdot)$ is a symbol function. $\boldsymbol{\varepsilon}$ is a gain matrix, in which the values of the diagonal elements can be adjusted by the fuzzy controller. There is the following relationship:

$$\begin{cases} \boldsymbol{M}_{eq\theta} = \boldsymbol{J}^{-\mathrm{T}}\boldsymbol{J}^{+}\boldsymbol{r}\boldsymbol{M}_{eq} \\ \boldsymbol{N}_{eq\theta} = \boldsymbol{J}^{-\mathrm{T}}\boldsymbol{J}^{+}\boldsymbol{r}\boldsymbol{N}_{eq} \\ \boldsymbol{G}_{eq\theta} = \boldsymbol{J}^{-\mathrm{T}}\boldsymbol{J}^{+}\boldsymbol{r}\boldsymbol{J}^{-\mathrm{T}}\boldsymbol{G}_{eq} \end{cases} \tag{21}$$

In order to prove the stability of the designed FSMVA control algorithm, a Lyapunov function is defined as follows:

$$V = \frac{1}{2}\boldsymbol{s}^{\mathrm{T}}(t)\boldsymbol{s}(t) \tag{22}$$

Combined with the first derivative of EQ. (21), and EQ. (21) can be arranged as:

$$\begin{aligned} \dot{V} &= \boldsymbol{s}^{\mathrm{T}}(t)\dot{\boldsymbol{s}}(t)\boldsymbol{s}^{\mathrm{T}}(t) \\ &= \left[\boldsymbol{K}\dot{\boldsymbol{e}}(t) + \ddot{\boldsymbol{\theta}}(t) - \boldsymbol{M}_{eq\theta}^{-1}(\boldsymbol{u}(t) + (\boldsymbol{N}_{eq\theta} - \boldsymbol{M}_{eq\theta}\boldsymbol{J}^{+}\dot{\boldsymbol{J}})\boldsymbol{\theta}(t)\right. \\ &\quad \left. -\boldsymbol{G}_{eq\theta} - \boldsymbol{W}_e + \boldsymbol{M}_{eq\theta}\boldsymbol{\varepsilon} \cdot \mathrm{sgn}(\boldsymbol{s}(t)))\right] \\ &= \boldsymbol{s}^{\mathrm{T}}(t)\left[-\boldsymbol{M}_{eq\theta}^{-1}(-\boldsymbol{W}_e + \boldsymbol{M}_{eq\theta}\boldsymbol{\varepsilon} \cdot \mathrm{sgn}(\boldsymbol{s}(t))\right] \\ &= \boldsymbol{s}^{\mathrm{T}}(t)\left[\boldsymbol{M}_{eq\theta}^{-1}\boldsymbol{W}_e - \boldsymbol{\varepsilon} \cdot \mathrm{sgn}(\boldsymbol{s}(t))\right] \\ &= \boldsymbol{s}^{\mathrm{T}}(t)\boldsymbol{M}_{eq\theta}^{-1}\boldsymbol{W}_e - \sum_{i=1}^{4}\varepsilon_i(s_i(t)) \end{aligned} \tag{23}$$

In addition, because the unknown external interference and modeling errors are bounded in actual application and meet the following condition:

$$\left|\boldsymbol{M}_{eq\theta}^{-1}\boldsymbol{W}_e\right| < \xi_u \tag{24}$$

Let $\xi_u \leq \varepsilon_i$, then EQ. (23) meets condition:

$$\dot{V} = \boldsymbol{s}^{\mathrm{T}}(t)\boldsymbol{M}_{eq\theta}^{-1}\boldsymbol{W}_e - \sum_{i=1}^{4}\varepsilon_i(s_i(t)) < \sum_{i=1}^{4}s_i(t)\left(\xi_u - \varepsilon_i\right) < 0 \tag{25}$$

One can be found from the above analysis that the Lyapunov function V is positive definite and $\dot{V}$ is negative definite. When $|\boldsymbol{s}(t)| \to \infty$, $V \to \infty$. According to the Lyapunov's stability discrimination theorem, the system with the closed-loop control strategy is asymptotically stable, and its equilibrium position is the system's asymptotic stability point in large-range.

The chattering phenomenon exists generally in the sliding mode control systems. By EQ. (20), the variation of symbol function is discrete, and the system will switch back and forth in near sliding surface $|\boldsymbol{s}| = 0$. The gain value $\boldsymbol{\varepsilon}$ directly affects the speed of approaching the sliding surface and dynamic quality of the system: under the premise of meeting the system stability condition $\xi_u \leq \varepsilon_i$, the gain value $\boldsymbol{\varepsilon}$ is too small, which increases the time that the system to reach the sliding surface and reduces the convergence speed of the system. On the contrary, the gain value $\boldsymbol{\varepsilon}$ is too large, which will increase the speed of the system to reach the sliding surface. The inertia of the system will make it cross the sliding surface, and the system's chattering phenomenon will be increased. In order to improve the dynamic performance of the system, the gain value $\boldsymbol{\varepsilon}$ needs to be optimized and adjusted according to the real-time state of the system.

Combined with the slope of the sliding surface $\boldsymbol{s}(t)$ and its change rate $\dot{\boldsymbol{s}}(t)$, a fuzzy controller is designed to optimize and

adjust the gain value $\boldsymbol{\varepsilon}$ of the sliding mode controller (SMC). The fuzzy controller can be designed as:

$$\varepsilon_i = \xi_u + \Delta\varepsilon_i = \xi_u + \mathrm{fuz}(s_i(t), \dot{s}_i(t)) \tag{26}$$

where $\Delta\varepsilon_i$ is adjustment amount of the gain value $\boldsymbol{\varepsilon}$. $\mathrm{fuz}(s_i(t), \dot{s}_i(t))$ represents a fuzzy operation.

The fuzzy rules used in this study are as follows:

(1) If $s_i(t) \cdot \dot{s}_i(t) > 0$, the status point of the system is moving away from the sliding surface. When the value $s_i(t)$ and $\dot{s}_i(t)$ is larger, the fuzzy control system should drive the motion state point of the system to return to the sliding surface as soon as possible by increasing the gain value $\boldsymbol{\varepsilon}$.

(2) If $s_i(t) \cdot \dot{s}_i(t) < 0$, the status point of the system is moving in the direction close to the sliding surface. When the value of $s_i(t)$ is too small or $\dot{s}_i(t)$ is too large, the fuzzy control system should drive the motion state point of the system to return to the sliding surface at a smaller speed by decreasing the gain value $\boldsymbol{\varepsilon}$, which can reduce the chattering phenomenon of the system.

In fuzzy control system, the inputs are clear values in form of crisp number. However, fuzzy controllers cannot recognize clear values. Therefore, they must be converted into linguistic variables through fuzzification [20]. A fuzzy control system is designed with the Mamdani fuzzy inference method to adjust the gain value $\boldsymbol{\varepsilon}$ in real-time. The normalized membership functions of $s_i(t)$, $\dot{s}_i(t)$ and $\Delta\varepsilon_i$ are shown in Fig. 4. All fuzzy subsets use Z-shaped, triangular, and S-shaped membership functions. The output and the inputs of the fuzzy control system are just the opposite. It is necessary to obtain the change of the control action, the output of the fuzzy

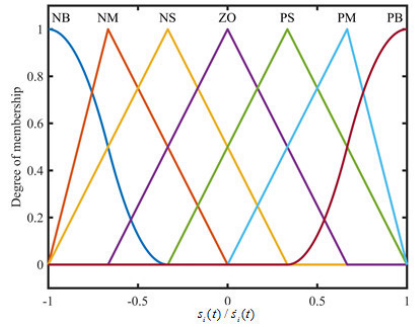

(a) $s_i(t) / \dot{s}_i(t)$

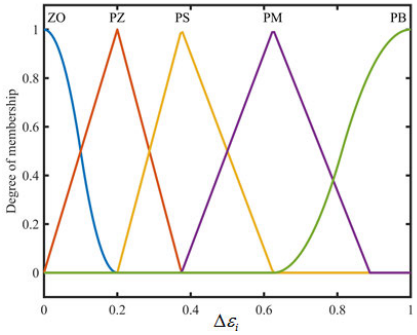

(b) $\Delta\varepsilon_i$

FIGURE 4. Normalized membership functions of $s_i(t)$, $\dot{s}_i(t)$ and $\Delta\varepsilon_i$.

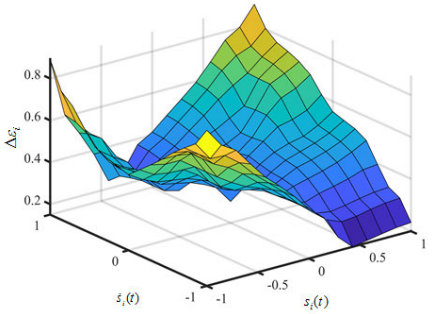

FIGURE 5. Relationship between the inputs and the output of fuzzy inference.

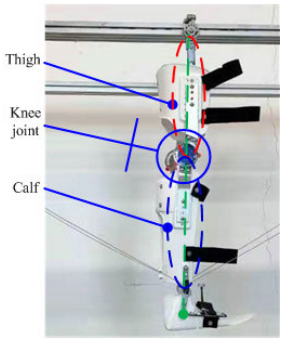

FIGURE 6. Prosthetic limb.

control system, with calculating based on the inputs using a fuzzy inference mechanism. The defuzzification converts the linguistic variable into a crisp value to adjust the gain value ε_i of the sliding mode controller in real-time.

The key of the fuzzy controller is inference. According to the membership function of the inputs, the expert knowledge will provide 49 fuzzy rules for control. The relationship between the inputs and the output of fuzzy inference is shown in Fig. 5. The fuzzy inference is realized with the Mamdani inference method.

V. EXPERIMENTAL RESEARCH

In order to verify the control effect of the proposed FSMVA controller for the CDLR, the trajectory tracking experiments with different admittance parameters are carried out on the experimental system of the CDLR. The flexion-extension motion trajectory of the human lower limbs in the sagittal plane is selected as the motion trajectory of the end-effector.

Considering safety and ethical issues, we use a prosthetic limb to simulate the lower limb of the patient for experimental research. The knee joint of this prosthetic limb is not equipped with a driving device, so the thigh and calf of the prosthetic limb are fixedly installed to make them collinear, as shown in Fig. 6.

Hence, the selected motion trajectory can be expressed as:

$$\begin{cases} x = x_0 \\ y = y_0 + (l_{\mathrm{thigh}} + l_{\mathrm{calf}}) \sin(\theta(t)) \\ z = z_0 - (l_{\mathrm{thigh}} + l_{\mathrm{calf}}) \cos(\theta(t)) \end{cases} \tag{27}$$

where (x_0, y_0, z_0) is the position of the hip joint. l_{thigh} and l_{calf} are the length of the thigh and the calf. $\theta(t)$ is the flexion-extension angle of the hip joint in the sagittal plane.

The trajectory tracking test experiment with different admittance parameters mainly includes three groups of experiments, which are the trajectory tracking experiment with no admittance, the trajectory tracking experiments with fixed admittances, and the trajectory tracking experiment with variable admittances based on safety evaluation and supervision. The trajectory tracking experiment with no admittances is performed to verify the position control performance of the proposed fuzzy sliding mode (FSM) controller. The trajectory tracking experiments with fixed admittances are performed to analyze the influence of the fixed admittance parameters on the trajectory tracking performance. The trajectory tracking experiment with variable admittances is performed to verify that the proposed FSMVA controller can adjust the admittance parameters of the admittance controller in real-time according to the system safety evaluation and supervision algorithm and the comprehensive evaluation of the patient's rehabilitation effect to adopt the training needs of patients in different rehabilitation stages.

A. TRAJECTORY TRACKING EXPERIMENT WITH NO ADMITTANCES

In the initial stage of the rehabilitation training, the training mode of the robot is mainly passive training mode. The CDLR should complete the training task by tracking the desired trajectory to prevent the muscle atrophy of lower limbs. In the control strategy block diagram shown in Fig. 3, when the outer loop admittance parameters of the admittance controller are all set to infinity (that is, no admittance control), the control system of the CDLR is transformed into a position controller (FSM controller) that tracks the desired trajectory. Therefore, the purpose of the trajectory tracking experiment with no admittance is to verify the control accuracy of the inner loop FSM controller.

Assume that the initial state of the test experiment is that the prosthetic limb is in a natural drooping state, that is, the hip joint angle $\theta(0) = 0°$, as shown in Fig.6. The parameters of a prosthetic limb ($l_{\text{thigh}} = 42.327$ cm, $l_{\text{calf}} = 39.681$ cm) are used in the following different experiments. The parameters of the FSMVA controller selected in this study are: $\boldsymbol{K} = diag[600, 600, 600, 600]$, $M_{da0} = M_{dp0} = 20^{10}$, $\alpha_a = \alpha_p = 0$, $B_{da0} = B_{dp0} = 20^{10}$, $\beta_a = \beta_p = 0$, $K_{da0} = K_{dp0} = 20^{10}$, and $\gamma_a = \gamma_p = 0$.

The experimental results of trajectory tracking with infinite admittance are shown in Fig. 7. It can be seen from the experimental data that the test experimental results can track the desired trajectory well, and the root mean square error of the experimental results RMSE = 3.87 mm and the mean error ME = 3.36 mm, which can meet the basic requirements of rehabilitation training. It indicates that the control accuracy of the FSM controller can meet the requirements of rehabilitation training. The change curve of cable tension is shown in Fig. 7(c), in the trajectory tracking with infinite admittances, and the change curve of the safety evaluation index of the tracking system is shown in Fig. 7(d). When external interference acts on the system in the training process, the system will adjust the cable tension to ensure the accuracy of the tracking trajectory.

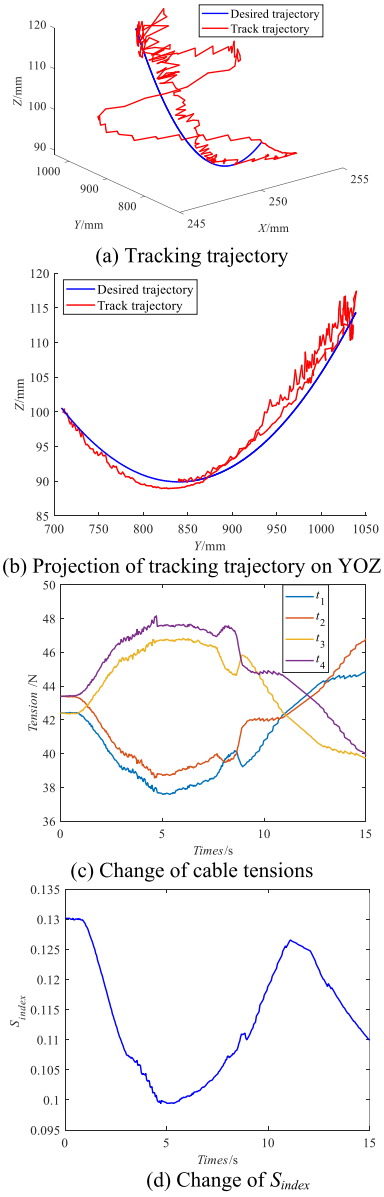

FIGURE 7. Experimental results of trajectory tracking with no admittance.

In Fig. 7(a), the display range of the X-axis is limited to [245, 255] mm. The maximum error value is 4.39 mm, in the X-axis direction, and the mean error is 1.56 mm.

B. TRAJECTORY TRACKING EXPERIMENT WITH FIXED ADMITTANCES

The passive training mode with no admittance is mainly suitable for patients without limb muscle strength to prevent muscle atrophy and muscle degeneration. However, the lower

limb muscles may recover part of the muscle strength after rehabilitation training for a period of time. Admittance control is introduced in passive training. By adjusting the admittance parameters, the compliance of human-machine interaction training can be improved to ensure the patient's comfort and safety during training. In order to analyze the influence of the FSMVA controller on the tracking trajectory performance with different admittances configurations, trajectory tracking experiments with three different admittances configurations (small admittance, medium admittance, and large admittance) are performed. During the experiment, the initial state of the trajectory tracking experiment is the same as the trajectory tracking experiment with no admittance. In addition, a constant vertical force (10N) is applied to the end-effector to simulate the human-machine interaction force. In the experiment, combined with the reference [40], the selected three different admittances configurations are shown in Tab. 1.

TABLE 1. Three different admittances configurations.

Admittances Configurations	M_d (N·s^2/mm)	B_d (N·s/mm)	K_d (N/mm)
Small admittance	*diag*[10, 10, 10, 10]	*diag*[0.2,0.2,0.2,0.2]	*diag*[5, 5, 5, 5]
Medium admittance	*diag*[15, 15, 15, 15]	*diag*[0.3,0.3,0.3,0.3]	*diag*[10,10,10,10]
Large admittance	*diag*[20, 20, 20, 20]	*diag*[1.0,1.0,1.0,1.0]	*diag*[15,15,15,15]

Fig. 8-10 show the experimental results of trajectory tracking with the admittance configurations of small admittance, medium admittance, and large admittance, respectively. The root mean square errors and the mean errors of the trajectory tracking with the small admittance configuration, medium admittance configuration, and large admittance configuration are shown in table 2. It can be seen that as the admittance parameters increase, the deviation of the tracking trajectory from the desired trajectory will be smaller. In addition, the safety evaluation index of the tracking experiments in three different admittance configurations hardly changed.

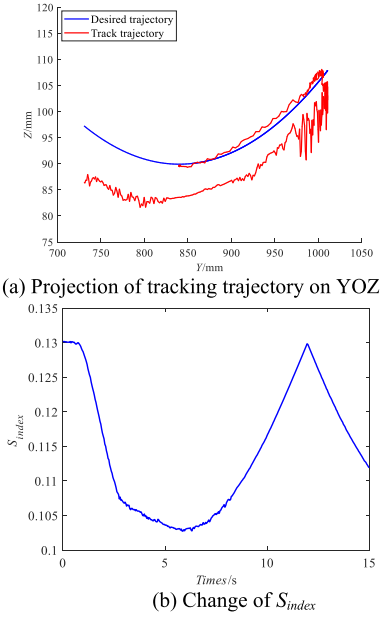

(a) Projection of tracking trajectory on YOZ

(b) Change of S_{index}

FIGURE 8. Experimental results of trajectory tracking with small admittance configuration.

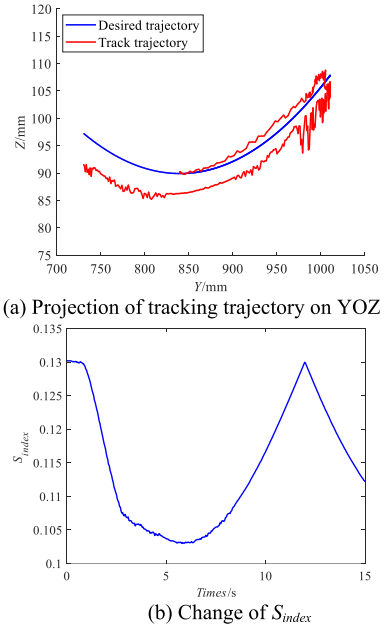

(a) Projection of tracking trajectory on YOZ

(b) Change of S_{index}

FIGURE 9. Experimental results of trajectory tracking with medium admittance configuration.

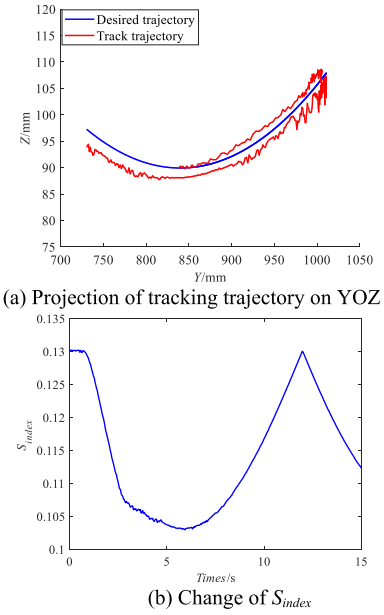

(a) Projection of tracking trajectory on YOZ

(b) Change of S_{index}

FIGURE 10. Experimental results of trajectory tracking with large admittance configuration.

C. TRAJECTORY TRACKING EXPERIMENT WITH VARIABLE ADMITTANCES

In actual rehabilitation training, for patients who have recovered part of their muscle strength, when the direction of the force provided by the lower limb is consistent with the

TABLE 2. Track trajectory error with fixed admittances.

Admittances Configurations	RMSE(mm)	ME(mm)
Small admittance	12.85	7.81
Medium admittance	8.47	526
Large admittance	4.29	2.88

movement direction of the desired trajectory, the training is regarded as a passive training mode. When the direction of the force provided by the lower limb is opposite to the movement direction of the desired trajectory, the training is regarded as an active training mode [40]. In order to improve the training effect in the active training mode, the system needs to reduce the error of trajectory tracking to increase the patient's active participation and training intensity. A larger admittance configuration needs to be selected in the active training mode. In the passive training mode, the patient's ability to provide resistance to the force of the robot is poorer, so the system is required to have high flexibility to improve the comfort and safety of patients in training. A smaller admittance configuration needs to be selected in the passive training mode. According to the experimental settings, since the direction of the simulated interaction force is opposite to the motion direction of the end-effector between 0-7.3 s, the training is the active training mode between 0-7.3 s. After 7.3 s, their directions are the same, and the training is set as the passive training mode after 7.3 s. Hence, the variable admittances configurations based on safety evaluation and supervision are shown in table 3.

TABLE 3. Variable admittance configurations of the FMSVA controller.

Training mode	M_{d0}	α	B_{d0}	β	K_{d0}	γ
Active training mode	30	5	5	2	10	3
Passive training mode	15	0.6	2	0.2	5	0.5

Fig. 11 shows the experimental results of trajectory tracking with the variable admittance configurations of the FMSVA controller based on the safety evaluation and supervision. It can be seen from the experimental data that RMSE is 5.54 mm and the ME is 2.65 mm. In addition, in the active training phase, the motion error between the tracking trajectory and the desired trajectory is small, and ME is 0.97 mm. However, in the passive training phase, the motion error between the tracking trajectory and the desired trajectory is larger, and ME is 3.86 mm. Fig. 11(b)-(c) respectively show the change curves of the cable tension and the safety evaluation index of the trajectory tracking experiment with the variable admittance configurations of the FMSVA controller. Fig. 11(d)-(f) show the change curves of the admittance configuration parameters M_d, B_d, and K_d, respectively. It can be seen that the admittance configuration parameters M_d, B_d, and K_d can change with the change of the safety evaluation index S_{static}, and their changing law is consistent. According to the adjustment algorithm of the admittance parameters of the admittance controller, EQ. (13), their change rules are right. Therefore, the proposed FSMVA controller can adjust the admittance configuration in real-time according to the safety evaluation index in the training process. In the active training process, the parameters of the admittance controller will increase, and the tracking error will reduce to improve the training intensity and effect of patients. In the passive training process, the parameters of the admittance controller will reduce, and the tracking error of the end-effector will increase to reduce the interaction force between the patient and the robot to ensure the safety of the patient.

Based on the analysis of the above trajectory tracking experiment results, it can be seen that the proposed FSMVA controller is more suitable for the rehabilitation training of patients in the whole rehabilitation phases than the fixed admittance controller. Hence, the comprehensive evaluation of the patient rehabilitation effect given by rehabilitation physiotherapists and the safety evaluation of the system is considered in the adjustment algorithm of the admittance parameters of the FSMVA controller, which can adjust the admittance configurations of the FSMVA controller in real-time. It can not only adjust the training intensity of the patient and improve the training effect according to the muscle strength of the patient's lower limbs in the active training process, but also increase the adjustment amount of the training trajectory according to the patient's training needs in the passive training process to further ensure the patient's safety and comfort. This study is different from other studies in two main aspects. Firstly, the safety evaluation and supervision mechanism is established according to the safety evaluation method of the CDLR system, and the admittance parameters of the FSMVA controller can be adjusted in real-time based on the safety evaluation index. Secondly, the different rehabilitation training plans given by rehabilitation physiotherapists, based on clinical experience and the comprehensive evaluation of the rehabilitation effects of different patients in the active training mode and passive training mode, are considered to further adjust and optimize the admittance parameters of the FSMVA controller. Therefore, this study reserves the adjustment parameters α_a, α_p, β_a, β_p, γ_a, and γ_p for the admittance controller in the adjustment algorithm of the admittance parameters.

In this study, the biggest advantage is that the safety of the system and the training needs of patients at different rehabilitation stages are considered in the rehabilitation training, and the admittance parameters of the FSMVA controller can be adjusted in real-time to improve the efficiency and safety of rehabilitation training. In the active training process, increasing the admittance parameters means increasing the stiffness and damping of the CDLR, and then the training intensity for the patient will be increased, which can effectively improve the patient's participation and enthusiasm. In the passive training process, decreasing the admittance parameter means decreasing the stiffness and damping of the CDLR (that is, the better the flexibility of the system), which can effectively

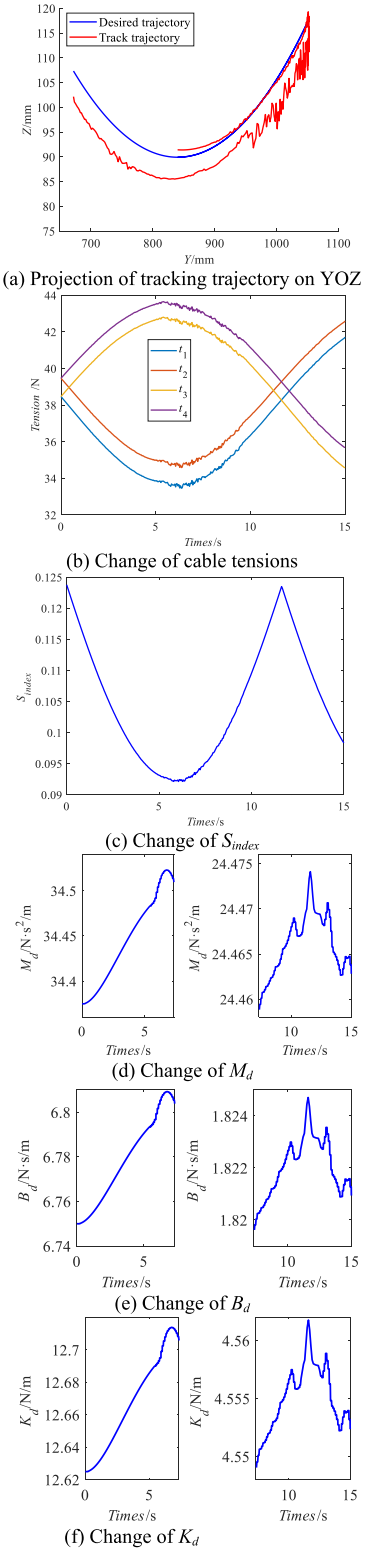

FIGURE 11. Experimental results of trajectory tracking with variable admittance configurations of the FMSVA controller.

improve the safety and comfort of patients during the training process.

Finally, it is worth noting that this study has one limitation. The adjustment algorithm of the admittance parameters of the variable admittance controller not only considers the safety of the CDLR system, but also takes into account the rehabilitation training needs of different patients in different rehabilitation stages. However, the influences of the adjustment parameters α_a, α_p, β_a, β_p, γ_a, and γ_p for the admittance controller, given by rehabilitation physiotherapists based on clinical experience and the comprehensive evaluation of the rehabilitation effects of different patients in the active training mode and passive training mode, on the rehabilitation training effect of patients are not discussed in the study. Therefore, future work needs to further improve and optimize the evaluation system of the robot-assisted patient in the rehabilitation training process based on the results of this research. Combined with the clinical experience and professional opinions of rehabilitation physiotherapists, the adjustment parameters α_a, α_p, β_a, β_p, γ_a, and γ_p of the admittance control for the FSMVA controller can be automatically configured in different rehabilitation stages and training courses to provide a basis for optimizing system control parameters and man-machine test experiments.

VI. CONCLUSION

A coordinated control strategy was presented in this paper based on the fuzzy sliding mode variable admittance control method for the CDLR system, which can adjust the control parameters of the admittance controller in real-time according to the system safety evaluation index and the comprehensive evaluation of the patient's rehabilitation effect. The derivation process of the fuzzy sliding mode variable admittance control algorithm was analyzed, and the stability of the system was proved based on the Lyapunov stability criterion. The trajectory tracking experiments with no admittance, fixed admittance, and variable admittance parameters based on safety evaluation and supervision were carried out on the experimental platform. The experimental results show that the proposed FSMVA controller has high position tracking ability and can meet the needs of lower limb rehabilitation training. In addition, the proposed FSMVA controller can automatically switch between active training mode and passive training mode, and adjust the control parameters of the admittance controller in real-time. Which can not only change the adjustment amount of motion trajectory according to the training needs of patients in passive training is to ensure the safety and comfort of the patient during the rehabilitation training process, but also adjust the admittance parameters of the admittance controller according to the patient's exercise ability during the active training process to increase the training intensity and efficiency.

Future work, based on the clinical experience and professional opinions of rehabilitation physiotherapists, the evaluation system of the robot-assisted patient in the rehabilitation training process will be further improved, which can automatically configure the adjustment parameters of the admittance control for the FSMVA controller in different rehabilitation stages and training processes of patients combined with the physiological parameters of patients, like

electromyogram (EMG). Human-machine compliance test experiments will be carried out.

ACKNOWLEDGMENT

The authors would like to thank the editors and reviewers for their instructive comments that helped to improve the quality of the paper.

REFERENCES

[1] I. Geonea, N. Dumitru, D. Tarnita, C. Copilusi, and A. S. Rosca, "New design and motion analysis of an exoskeleton robot for assisting human locomotion," in *Proc. 22nd IEEE Int. Conf. Automat., Qual. Test., Robot. (AQTR)*, May 2020, pp. 201–206.

[2] Y.-L. Wang, K.-Y. Wang, W.-L. Wang, P.-C. Yin, and Z. Han, "Appraise and analysis of dynamical stability of cable-driven lower limb rehabilitation training robot," *J. Mech. Sci. Technol.*, vol. 33, no. 11, pp. 5461–5472, Nov. 2019.

[3] R. Bertani, C. Melegari, M. C. De Cola, A. Bramanti, P. Bramanti, and R. S. Calabrò, "Effects of robot-assisted upper limb rehabilitation in stroke patients: A systematic review with meta-analysis," *Neurol. Sci.*, vol. 38, no. 9, pp. 1561–1569, Sep. 2017.

[4] Y.-L. Wang, K.-Y. Wang, W.-L. Wang, Z. Han, and Z.-X. Zhang, "Appraisement and analysis of dynamical stability of under-constrained cable-driven lower-limb rehabilitation training robot," *Robotica*, vol. 39, no. 6, pp. 1023–1036, Jun. 2021, doi: 10.1017/S0263574720000879.

[5] S.-H. Chen, W.-M. Lien, W.-W. Wang, G.-D. Lee, L.-C. Hsu, K.-W. Lee, S.-Y. Lin, C.-H. Lin, L.-C. Fu, J.-S. Lai, J.-J. Luh, and W.-S. Chen, "Assistive control system for upper limb rehabilitation robot," *IEEE Trans. Neural Syst. Rehabil. Eng.*, vol. 24, no. 11, pp. 209–1199, Nov. 2016.

[6] B. Ugurlu, M. Nishimura, K. Hyodo, M. Kawanishi, and T. Narikiyo, "Proof of concept for robot-aided upper limb rehabilitation using disturbance observers," *IEEE Trans. Human-Machine Syst.*, vol. 45, no. 1, pp. 110–118, Feb. 2015.

[7] X. Cui, W. Chen, X. Jin, and S. K. Agrawal, "Design of a 7-DOF cable-driven arm exoskeleton (CAREX-7) and a controller for dexterous motion training or assistance," *IEEE/ASME Trans. Mechatronics*, vol. 22, no. 1, pp. 161–172, Feb. 2017.

[8] N. Aliman, R. Ramli, and S. M. Haris, "Design and development of lower limb exoskeletons: A survey," *Robot. Auton. Syst.*, vol. 95, pp. 102–116, Sep. 2017.

[9] M. S. Amiri, R. Ramli, M. A. A. Tarmizi, and M. F. Ibrahim, "Simulation and control of a six degree of freedom lower limb exoskeleton," *J. Kejuruteraan*, vol. 32, no. 2, pp. 197–204, May 2020.

[10] A. L. Ármannsdóttir, P. Beckerle, J. C. Moreno, E. H. F. van Asseldonk, M.-T. Manrique-Sancho, A. J. Del-Ama, J. F. Veneman, and K. Briem, "Assessing the involvement of users during development of lower limb wearable robotic exoskeletons: A survey study," *Hum. Factors, J. Hum. Factors Ergonom. Soc.*, vol. 62, no. 3, pp. 351–364, May 2020.

[11] R. W. Nuckols, K. Z. Takahashi, D. J. Farris, S. Mizrachi, R. Riemer, and G. S. Sawicki, "Mechanics of walking and running up and downhill: A joint-level perspective to guide design of lower-limb exoskeletons," *PLoS ONE*, vol. 15, no. 8, Aug. 2020, Art. no. e0231996.

[12] X. Jin, A. Prado, and S. K. Agrawal, "Retraining of human gait-are lightweight cable-driven leg exoskeleton designs effective?" *IEEE Trans. Neural Syst. Rehabil. Eng.*, vol. 26, no. 4, pp. 847–855, Apr. 2018.

[13] H. J. Hong, J. Ali, and L. Ren, "A review on topological architecture and design methods of cable-driven mechanism," *Adv. Mech. Eng.*, vol. 10, no. 5, pp. 1–14, May 2018.

[14] H. Kino, T. Yoshitake, R. Wada, K. Tahara, and K. Tsuda, "3-DOF planar parallel-wire driven robot with an active balancer and its model-based adaptive control," *Adv. Robot.*, vol. 32, no. 14, pp. 766–777, Jul. 2018.

[15] S. Qian, B. Zi, W.-W. Shang, and Q. S. Xu, "A review on cable-driven parallel robots," *Chin. J. Mech. Eng.*, vol. 31, no. 1, pp. 66–77. Dec. 2018.

[16] Y. Zou, N. Wang, X. Wang, H. Ma, and K. Liu, "Design and experimental research of movable cable-driven lower limb rehabilitation robot," *IEEE Access*, vol. 7, pp. 2315–2326, 2019.

[17] Y. Zou, K. Liu, N. Wang, J. Li, X. Geng, and K. Chang, "Design and optimization of movable cable-driven lower-limb rehabilitation robot," in *Proc. 3rd Int. Conf. Adv. Robot. Mechatronics (ICARM)*, Jul. 2018, pp. 714–719.

[18] G. Zuccon, M. Bottin, M. Ceccarelli, and G. Rosati, "Design and performance of an elbow assisting mechanism," *Machines*, vol. 8, no. 4, p. 68, Oct. 2020.

[19] M. Russo and M. Ceccarelli, "Analysis of a wearable robotic system for ankle rehabilitation," *Machines*, vol. 8, no. 3, p. 48, Aug. 2020.

[20] Q. Chen, B. Zi, Z. Sun, Y. Li, and Q. Xu, "Design and development of a new cable-driven parallel robot for waist rehabilitation," *IEEE/ASME Trans. Mechatronics*, vol. 24, no. 4, pp. 1497–1507, Aug. 2019.

[21] D. Cafolla, M. Russo, and G. Carbone, "CUBE, a cable-driven device for limb rehabilitation," *J. Bionic Eng.*, vol. 16, no. 3, pp. 493–502, May 2019.

[22] Y.-L. Wang, K.-Y. Wang, Z.-X. Zhang, Z. Han, and W.-L. Wang, "Analysis of dynamical stability of rigid-flexible hybrid-driven lower limb rehabilitation robot," *J. Mech. Sci. Technol.*, vol. 34, no. 4, pp. 1735–1748, Apr. 2020.

[23] K.-Y. Wang, P.-C. Yin, H.-P. Yang, S. Wang, and X.-Q. Tang, "The man-machine motion planning of rigid-flexible hybrid lower limb rehabilitation robot," *Adv. Mech. Eng.*, vol. 10, no. 6, pp. 1–11, Jun. 2018.

[24] L. Zhang, L. Li, Y. Zou, K. Wang, X. Jiang, and H. Ju, "Force control strategy and bench press experimental research of a cable driven astronaut rehabilitative training robot," *IEEE Access*, vol. 5, pp. 9981–9989, 2017.

[25] Y. Wang, K. Wang, Z. Zhang, and Z. Mo, "Control strategy and experimental research of a cable-driven lower limb rehabilitation robot," *Proc. Inst. Mech. Eng., C, J. Mech. Eng. Sci.*, pp. 1–14, Aug. 2020, doi: 10.1177/0954406220952510.

[26] S. Mefoued, "A robust adaptive neural control scheme to drive an actuated orthosis for assistance of knee movements," *Neurocomputing*, vol. 140, pp. 27–40, Sep. 2014.

[27] C. Jarrett and A. J. McDaid, "Robust control of a cable-driven soft exoskeleton joint for intrinsic human-robot interaction," *IEEE Trans. Neural Syst. Rehabil. Eng.*, vol. 25, no. 7, pp. 976–986, Jul. 2017.

[28] J. Niu, Q. Yang, X. Wang, and R. Song, "Sliding mode tracking control of a wire-driven upper-limb rehabilitation robot with nonlinear disturbance observer," *Frontiers Neurol.*, vol. 8, p. 511, Dec. 2017.

[29] H. L. Wei, Y. Y. Qui, and Y. Sheng, "Motion stable control for cable-driven parallel camera robots with high speeds," *J. Xidian Univ.*, vol. 43, no. 5, pp. 63–69 and 104, Oct. 2016.

[30] A. U. Pehlivan, D. P. Losey, and M. K. Omalley, "Minimal assist-as-needed controller for upper limb robotic rehabilitation," *IEEE Trans. Robot.*, vol. 32, no. 1, pp. 113–124, Feb. 2016.

[31] S. K. Banala, S. H. Kim, S. K. Agrawal, and J. P. Scholz, "Robot assisted gait training with active leg exoskeleton (ALEX)," *IEEE Trans. Neural Syst. Rehabil. Eng.*, vol. 17, no. 1, pp. 2–8, Feb. 2009.

[32] J. Jun, X. Jin, A. Pott, S. Park, J.-O. Park, and S. Y. Ko, "Hybrid position/force control using an admittance control scheme in Cartesian space for a 3-DOF planar cable-driven parallel robot," *Int. J. Control, Autom. Syst.*, vol. 14, no. 4, pp. 1106–1113, Aug. 2016.

[33] M. H. Korayem, M. Bamdad, H. Tourajizadeh, A. H. Korayem, and S. Bayat, "Analytical design of optimal trajectory with dynamic load-carrying capacity for cable-suspended manipulator," *Int. J. Adv. Manuf. Technol.*, vol. 60, nos. 1–4, pp. 317–327, Apr. 2012.

[34] M. H. Korayem, H. Tourajizadeh, and M. Bamdad, "Dynamic load carrying capacity of flexible cable suspended robot: Robust feedback linearization control approach," *J. Intell. Robot. Syst., Theory Appl.*, vol. 60, nos. 3–4, pp. 341–363, Dec. 2010.

[35] M. H. Korayem, H. Tourajizadeh, A. Zehfroosh, and A. H. Korayem, "Optimal path planning of a cable-suspended robot with moving boundary using optimal feedback linearization approach," *Nonlinear Dyn.*, vol. 78, no. 2, pp. 1515–1543, Oct. 2014.

[36] M. Rahmani and M. H. Rahman, "An upper-limb exoskeleton robot control using a novel fast fuzzy sliding mode control," *J. Intell. Fuzzy Syst.*, vol. 36, no. 3, pp. 2581–2592, Mar. 2019.

[37] A. Fortin-Cote, P. Cardou, and C. Gosselin, "An admittance control scheme for haptic interfaces based on cable-driven parallel mechanisms," in *Proc. IEEE Int. Conf. Robot. Automat. (ICRA)*, May 2014, pp. 819–825.

[38] Q. Yang, J. Niu, and R. Song, "Admittance control of a 3-DOF cable-driven rehabilitation robot for upper-limb in three dimensional workspace," in *Proc. 2nd Int. Conf. Adv. Robot. Mechatronics (ICARM)*, Aug. 2017, pp. 445–449.

[39] Y.-L. Wang, K.-Y. Wang, and Z.-X. Zhang, "Design, comprehensive evaluation, and experimental study of a cable-driven parallel robot for lower limb rehabilitation," *J. Brazilian Soc. Mech. Sci. Eng.*, vol. 42, no. 7, p. 371, Jun. 2020.

[40] Y. Tu, A. Zhu, J. Song, H. Shen, Z. Shen, X. Zhang, and G. Cao, "An adaptive sliding mode variable admittance control method for lower limb rehabilitation exoskeleton robot," *Appl. Sci.*, vol. 10, no. 7, p. 2536, Apr. 2020.
[41] Y. L. Wang, K. Y. Wang, K. C. Wang, and Z. J. Mo, "Safety evaluation and experimental study of a new bionic muscle cable-driven lower limb rehabilitation robot," *Sensors*, vol. 20, no. 24, p. 7020, Dec. 2020.

YAN-LIN WANG received the B.S. and M.S. degrees in mechatronic engineering from Lanzhou Jiaotong University, in 2014 and 2017, respectively. He is currently pursuing the Ph.D. degree with the College of Mechanical and Electrical Engineering, Harbin Engineering University, Harbin, China. His research interests include parallel robots, multi-robots systems, and cable-driven rehabilitation robots.

KE-YI WANG received the Ph.D. degree from the College of Mechanical and Electrical Engineering, Harbin Engineering University, in 2009. He is currently an Associate Professor with the College of Mechanical and Electrical Engineering, Harbin Engineering University. His current research interests include rehabilitation robot, parallel robot, and mechatronics.

XIANG LI received the B.S. degree from Beihua University, in 2014, and the M.S. degree from Jilin University, in 2017. She is currently pursuing the Ph.D. degree with the College of Mechanical and Electrical Engineering, Harbin Engineering University, Harbin, China. Her research interests include parallel robots and rehabilitation robots.

ZONG-JUN MO received the B.S. degree in mechanical manufacturing and automation from Harbin Engineering University, in 2019, where he is currently pursuing the M.S. degree in mechanical engineering. His research interests include cable driven robot and remote control systems.

KUI-CHENG WANG received the bachelor's degree in mechanical and electronic engineering from Huazhong Agricultural University, in 2018. He is currently pursuing the master's degree with the College of Mechanical and Electrical Engineering, Harbin Engineering University, Harbin, China. His research interest includes mechatronics design of flexible drive robot.